Alternative Prion Structural Changes Revealed by High Pressure†

Joan Torrent,‡,§ Maria Teresa Alvarez-Martinez,§ Frédéric Heitz,|| Jean-Pierre Liautard,§ Claude Balny,‡ and Reinhard Lange*,‡

INSERM U128, 1919 Route de Mende, F-34293 Montpellier cedex 5, France, INSERM U431, IFR 56, Place Eugène Bataillon, F-34095 Montpellier Cedex 5, France, and CRBM, CNRS-UPR 1086, IFR24, 1919 Route de Mende, F-34293 Montpellier Cedex 5, France

Received October 11, 2002; Revised Manuscript Received November 21, 2002

ABSTRACT: At high temperature, recombinant hamster prion protein ($SHaPrP_{90-231}$) undergoes aggregation and changes from a predominantly α-helical to β-sheet conformation. We then applied high pressure (200 MPa) to the β-sheet-rich conformation. The aggregation was reversed, and the original tertiary and secondary structures were recovered at ambient pressure, after pressure release. The application of a pressure of 200 MPa thus allowed studying the heat-induced equilibrium refolding in the absence of protein aggregation. Prion protein unfolding as a function of high pressure was also investigated. Simple two-state, reversible unfolding transitions were observed, as monitored by spectral changes in the UV and fluorescence of the hydrophobic probe 8-anilino-1-naphthalene sulfonate. However, these heat- and pressure-induced conformers differed in their unfolding free energy. At pressures over 400 MPa, strong thioflavin-T binding was observed, suggesting a further structural change to a metastable oligomeric structure.

Protein misfolding and aggregation are principal characteristics of a variety of neurodegenerative diseases (often associated with amyloidoses), including those induced by prions. Moreover, the misfolded isoform (PrP^{sc})[1] of the normal cellular prion protein (PrP^{c}) has been proposed as the sole component responsible for both pathology and infectivity in transmissible spongiform encephalopathies (TSE) (*1*). Under this hypothesis, self-propagating conformational rearrangement to a β-sheet-rich structure leads finally to the formation of proteinase K resistant aggregates in the form of β-amyloid fibrils (*2*, *3*). Clearly, an understanding of the molecular basis of these structural changes is required. Many experimental approaches, including the use of high temperature, chemical denaturants, salts, and extreme conditions of pH have shown that PrP can adopt completely different non-native conformational states (*4*−*8*) that may or may not proceed to formation of aggregates. However, despite many efforts using recombinant protein to induce in vitro formation of a PrP^{sc}-like state capable of causing neuronal degeneration and disease, no successful result has yet been obtained. The reason for this setback may be that the experimental conditions used so far do not lead to the alternative folded form associated with infectivity.

To address this issue, we investigated the use of high pressure as an alternative to find new pathways for prion structural changes. Recently, evidence that pressure may provide us with a better understanding of the folding−unfolding pathways of prions has already been reported in our laboratory using yeast prion protein Ure2 (*9*). The pressure response of a protein is directed by the volume change of the protein−solvent system, which is associated with conformational changes such as partial or complete protein unfolding or protein aggregation (*10*, *11*). High pressure shifts the conformational transition of a protein (*12*−*15*), often in a reversible manner, toward the state that occupies the smaller volume, which sometimes exhibits the characteristics of a molten globule-like structure (*16*−*22*). Such a perturbation takes place by favoring the dissociation of electrostatic bonds and by favoring the solvation of hydrophobic residues (*23*). The pathway induced by high pressure may be different than that under high temperature or in the presence of chaotropic agents. Furthermore, the application of moderate pressures has been shown, in certain cases, to protect unfolded proteins from aggregation and to assist disaggregation of protein aggregates (*24*−*26*). The reason for this structural effect of pressure can be understood as resulting from the hydration of buried hydrophobic residues (*27*, *28*).

In the present work, we report aggregation−disaggregation and protein structural changes of a recombinant mammalian PrP ($SHaPrP_{90-231}$) as a function of both pressure and temperature. The combination of different spectroscopic techniques shows that pressure and temperature act in different ways on both PrP structural changes and aggregation. Moreover, they reveal several alternative prion structural changes, which differ from those that have been observed by more conventional methods.

† Supported by GIS−prions (Ministery of Research), ATC−prions (INSERM), and Human Science Frontier Program (HSFP). J.T. acknowledges an INSERM Poste-Vert fellowship. M.T.A. was supported by a GIS−prions fellowship (Ministry of Research, France).

* Corresponding author. Tel: +33.467.613.365. Fax: +33.467.523.681. E-mail: lange@montp.inserm.fr.

‡ INSERM U128.

§ INSERM U431.

|| CRBM.

[1] Abbreviations: PrP, prion protein; PrP^{C}, cellular isoform; PrP^{Sc}, pathogenic isoform; $ShaPrP_{90-231}$, Syrian hamster recombinant PrP consisting of residues 90−231; ANS, 8-anilino-1-naphthalene sulfonate; FTIR, Fourier transform infrared.

10.1021/bi0269916 CCC: $25.00
Published on Web 01/16/2003

EXPERIMENTAL PROCEDURES

Prion Protein. The gene encoding $SHaPrP_{90-231}$ (the unglycosylated recombinant Syrian hamster PrP expanding from residues 90−231, corresponding to the sequence of the PK-resistant core of PrP^{sc}) was obtained from the construction plngPrP (kindly provided by Prof. Prusiner) (*29*). The design, cloning, and overexpression of the gene, as well as the protein purification procedure, will be described in detail elsewhere. Protein purity and homogeneity were verified by SDS−PAGE and immunoblotting, as well as reversed-phase HPLC using a 214TP10415 C4 column (Vydac). The protein was shown to be of the expected molecular weight by ES/MS (electrospray mass spectrometry) on a VG Bio-Q quadrupole with a mass range of 4000 Da (Bio-Tech). Proteins were stored at −20 °C in ultrapure water containing 0.005% sodium azide. This storage procedure had no effect on protein conformation or its tendency to aggregate. Protein concentration was determined spectrophotometrically using a molar extinction coefficient at 278 nm of 25 327 M^{-1} cm^{-1}.

Structural Characterization at Environmental Conditions. Circular Dichroism (CD) Spectroscopy. CD spectra were recorded at ambient conditions using a J810 spectropolarimeter (Jasco). A 0.1-cm optical path length quartz cell was used to record spectra of proteins in the far UV region (190−260 nm). Protein concentration and buffers were those used in the UV absorbance experiments. Baseline corrected CD spectra were acquired at a scan speed of 20 nm min^{-1}, a 1-nm bandwidth, and a response time of 1 s. The sample compartment was purged with pure dry nitrogen. Spectra were signal-averaged over four scans.

FTIR Spectroscopy. FTIR spectra were recorded at ambient conditions on an IFS28 spectrometer equipped with a DTGS detector (Bruker). The spectra (100 scans accumulation) were recorded at a spectral resolution of 2 cm^{-1} and analyzed (OPUS/IR2 program). For a comparison of soluble and aggregated protein, all spectra were recorded with dry samples. A comparison of dried protein and sample in solution did not reveal significant changes in their FTIR spectra (*29, 30*). Samples were prepared by protein deposition onto a fluorine plate, where the solvent was allowed to evaporate overnight at room temperature. The complex spectral contour observed for amide I and II bands was decomposed using a second-derivative method for the determination of the band positions that are assigned to different secondary structure elements (*31*).

Congo Red Staining and Birefringence. Aggregated protein suspension in 20 mM sodium phosphate buffer, pH 7.0, was air-dried on a glass microscope slide. The protein film was immersed in a solution containing 2% (w/v) Congo red and 80% (v/v) ethanol/water for 15 min and then rinsed by immersion in 90% ethanol for 2 min and dried. Birefringence was observed with a Leica DM IRM light microscope (Leica Microsystemes) equipped with a polarizer.

Structural Characterization at High Pressure or High Temperature. UV Absorbance Spectroscopy. For high-pressure experiments, the proteins were dissolved in 20 mM Tris-HCl buffer at pH 7.0. For experiments as a function of temperature, they were dissolved in 20 mM sodium phosphate buffer, pH 7.0. These buffers were selected for their relatively small pressure and thermal pH dependencies, respectively (*32*). The final protein concentration was 0.5 mg mL^{-1}, unless stated otherwise. Absorbance spectra between 260 and 305 nm were recorded in steps of 0.1 nm (1-nm bandpath) as a function of temperature and pressure, using a modified Cary3 (Varian) absorption spectrometer (*33*). Following each pressure or temperature change, typically in steps of 20 MPa or 3 °C, the sample was allowed to equilibrate for 6 min before the next measurement. Each spectrum was corrected for pressure and temperature dependence of the sample volume, and the fourth derivative spectra were determined as previously described (*33*, *34*). Transitions between two spectral forms were quantified by cumulative difference amplitude (CDA) as reported (*35*).

Fluorescence Spectroscopy. Fluorescence emission spectra were recorded on an Aminco-Bowmann Series 2 luminescence spectrometer (SLM Aminco), modified to accommodate a thermostated pressure cell. 1-Anilinonaphthalene-8-sulfonic acid (ANS) and thioflavin-T were used as extrinsic fluorescence probes. ANS is used to measure changes in the surface hydrophobicity of proteins. The increase in fluorescence intensity reflects the ANS-binding to clustered hydrophobic residues (*36*). Thioflavin-T is a dye used to detect amyloids (*37*). For ANS binding studies, fluorescence was excited (4-nm slit) at 350 nm, and emission spectra (2-nm slit) were collected (accumulation of five scans) between 420 and 575 nm. The final ANS concentration was 750 μM, and the protein concentration was 0.8 mg mL^{-1}. Samples were allowed to reach equilibrium for 5 min before data collection. For thioflavin-T, assays were performed by adding a freshly prepared stock solution to the protein samples to a final thioflavin-T concentration of 20 μM. A final PrP concentration of 0.3 mg mL^{-1} was used throughout. Fluorescence emission spectra were obtained with an excitation wavelength of 442 nm and excitation and emission slits of 4 and 8 nm, respectively.

Light Scattering Measurements. Kinetics. Protein aggregation−disaggregation was followed by monitoring the changes in light scattering intensity at 340 nm (16-nm slit widths) using an Aminco-Bowmann Series 2 luminescence spectrometer (SLM Aminco) modified to accommodate a thermostated pressure cell. Aggregation and disaggregation kinetics were induced by pressure-jumps at 70 °C; disaggregation experiments were also performed at 25 °C. For that, a homemade pressure-jump device was connected to the high pressure cell in the spectrofluorimeter. Pressure-jumps were carried out by opening an electrically driven pneumatic valve (Top Indrustries) localized between two pressure cells. The pressure-jumps consisted of sudden changes of pressure (typically 30 MPa) within a pressure range of 0.1−600 MPa. Such small pressure jumps induce a change in pH of less than 0.1 pH unit (*32*). The dead time of positive (upward) and negative (downward) pressure-jumps was 5 ms. The protein concentration was 0.3 mg mL^{-1} in 20 mM sodium phosphate buffer, pH 7.0. Changes in light scattering intensity as a function of time were fitted to single-exponential equations.

RESULTS

Temperature and Pressure Dependent Protein Aggregation. When $SHaPrP_{90-231}$ solutions at pH 7.0 were heated to a temperature higher than 57 °C, protein aggregation and large-scale precipitation took place. This process was re-

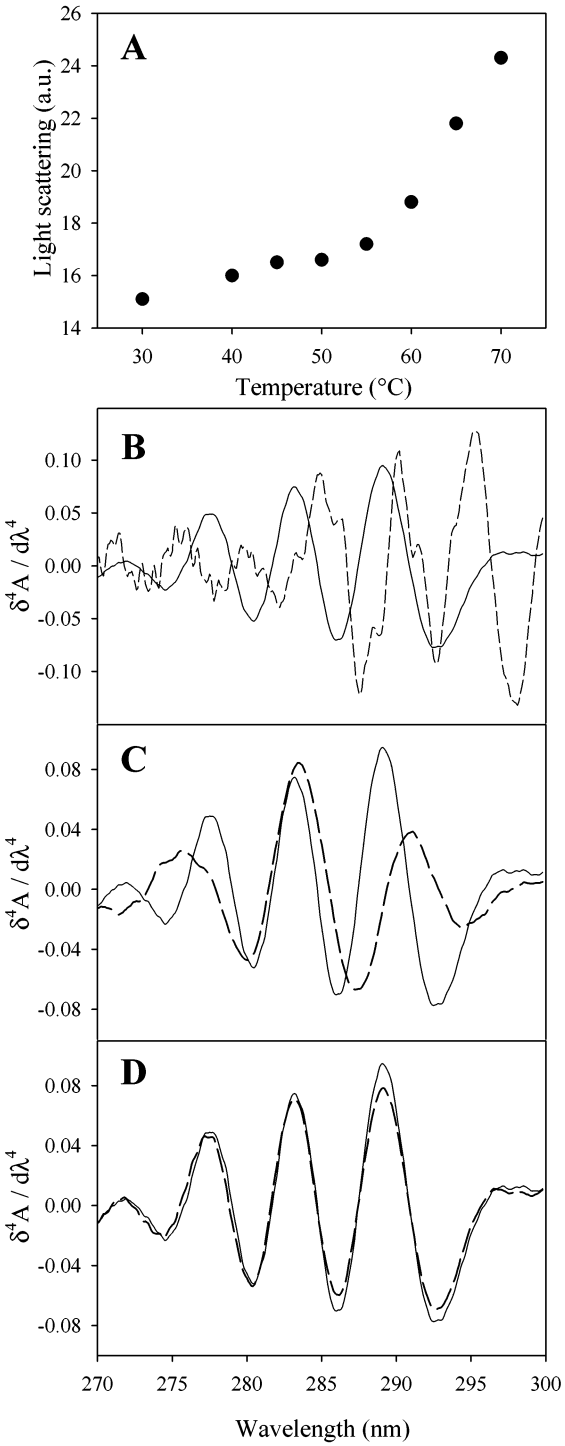

FIGURE 1: Aggregation, disaggregation, and refolding of $SHaPrP_{90-231}$. (A) Temperature-induced aggregation of the protein as measured by light scattering at 340 nm. (B, C, and D) Fourth derivative UV spectra of the protein under distinct pressure and temperature conditions. Shown for comparison is the fourth derivative UV spectrum of the native protein (solid line). Dashed lines depict (B) the aggregated protein formed after incubation of the sample at 70 °C; (C) the recovered soluble and unfolded protein after pressurization of the aggregates to 200 MPa for 25 min at 70 °C; and (D) the native protein obtained after decreasing temperature to 25 °C and releasing pressure. Solution conditions: protein at 0.5 mg mL^{-1} in sodium phosphate buffer, 20 mM, pH 7.0.

flected by a sharp increase in light scattering intensity (Figure 1A). The aggregates persisted once the sample was cooled to 25 °C. However, this aggregation process was reversed

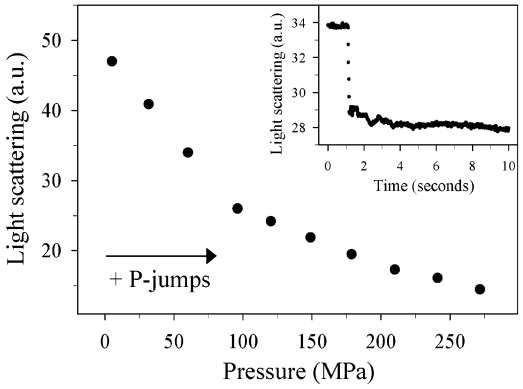

FIGURE 2: Pressure-induced disaggregation of $SHaPrP_{90-231}$ aggregates monitored by light scattering intensity at 340 nm at 70 °C. The inset shows a typical relaxation profile after a pressure-jump between 60 and 95 MPa. The protein concentration was 0.3 mg mL^{-1} in sodium phosphate buffer, 20 mM, at pH 7.0.

by applying a moderate pressure (200 MPa). After decreasing temperature and pressure release, the UV spectrum of native PrP was recovered (Figure 1B−D). CD and FTIR spectroscopy further confirmed full recovery of the native structure.

Kinetics of Protein Aggregation and Disaggregation. The kinetics of protein disaggregation were studied at 70 °C (conditions where aggregation is highly favored) after sudden increases of pressure in steps of 30 MPa, from atmospheric pressure to 275 MPa (Figure 2); reaggregation was followed at 70 °C by downward pressure-jumps. Each pressure-jump produced single exponential kinetics leading to a new equilibrium of light scattering intensity. The inset of Figure 2 shows a typical relaxation profile after a positive pressure-jump. Assuming in a first approximation that aggregation is linearly related to the intensity of scattered light, we evaluated the relaxation times for disaggregation and aggregation in the pressure range from 50 to 275 MPa as approximately 100 ms. Since the protein remained aggregated at atmospheric pressure when the temperature was lowered to room temperature, it was possible to record the disaggregation kinetics, by positive pressure jumps, at lower temperatures. However, the kinetics did not depend significantly on temperature between 25 and 70 °C.

Protein Structural Changes Accompanying Aggregation and Disaggregation. Changes in protein secondary structure of $SHaPrP_{90-231}$ accompanying protein aggregation and disaggregation were assessed by FTIR spectral analysis of amide I and II bands (Figure 3A). Second derivative analysis (Figure 3B) revealed that the major contribution corresponds to the α-helical form (1655 cm^{-1}), which is known to be the major structural component of $SHaPrP_{90-231}$ (*38*, *39*). Interestingly, the spectrum of the aggregated protein formed at 70 °C showed a strong enhancement of the 1620 cm^{-1} component, concomitant with a relative decrease of the 1655 cm^{-1} component. The 1620 cm^{-1} component, associated with the weak 1680 cm^{-1}, can be assigned to an antiparallel *β*-sheet structure, suggesting intermolecular association (*31*, *40*). The behavior of the amide II band that shifted from 1546 to 1540 cm^{-1} is also in line with the above-mentioned conformational transition. However, the prion sample that had been disaggregated by pressure showed no significant differences in amide I and II spectral outlines to that of the native protein. This was also confirmed by far UV CD analysis (results not shown). It is therefore clear that pressure

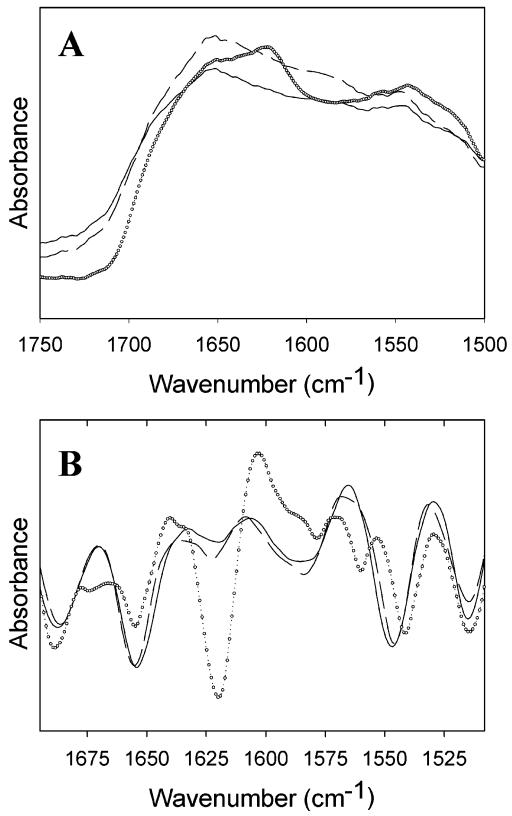

FIGURE 3: Fourier deconvoluted IR spectra of amide I and II bands of $SHaPrP_{90-231}$. (A) Zero order spectra. (B) Second derivative spectra. The solid lines represent native protein. Dotted lines depict the aggregated protein formed after incubation at 70 °C for 30 min. Dashed lines show the recovered soluble protein after pressurization of the aggregates at 200 MPa for 25 min at 70 °C. After each treatment, samples were lyophilized and resuspended in ultrapure water. The spectra were recorded after drying the samples overnight at room temperature.

not only reverses prion aggregation, but it also reverses the secondary structural changes that accompanied the aggregation process.

To determine potential amyloidogenic features of the aggregated protein obtained under high temperature (70 °C), a Congo red dye-binding assay was carried out. This exhibited the presence of some amyloid-like structures, as it was concluded from a blue-green birefringence observed under polarized light.

Temperature- and Pressure-Induced Conformational Changes Upon Protein Unfolding in the Absence of Aggregation. UV absorbance spectroscopy in the fourth derivative mode was used to evaluate prion conformational changes in the vicinity of tyrosine and tryptophan residues, as a function of pressure and temperature in the absence of protein aggregation. The analysis at high temperature (up to 80 °C) was possible by maintaining a constant pressure of 200 MPa, which prevented protein aggregation. High temperature (up to 80 °C, at 200 MPa) and high pressure (up to 480 MPa, at 40 °C) led to the same UV absorbance changes in the fourth derivative mode (Figure 4): a 1-nm red shift of the 289.6 nm band, a 1.5-nm blue shift of the 277.7 nm band, and no variation of the central peak at 283.4 nm. At 6 M guanidinium hydrochloride, similar shifts for these three major derivative bands were observed (results not shown).

Pressure- and heat-induced spectral changes were cooperative, showing clear isosbestic points at 276.8 and 290.8 nm,

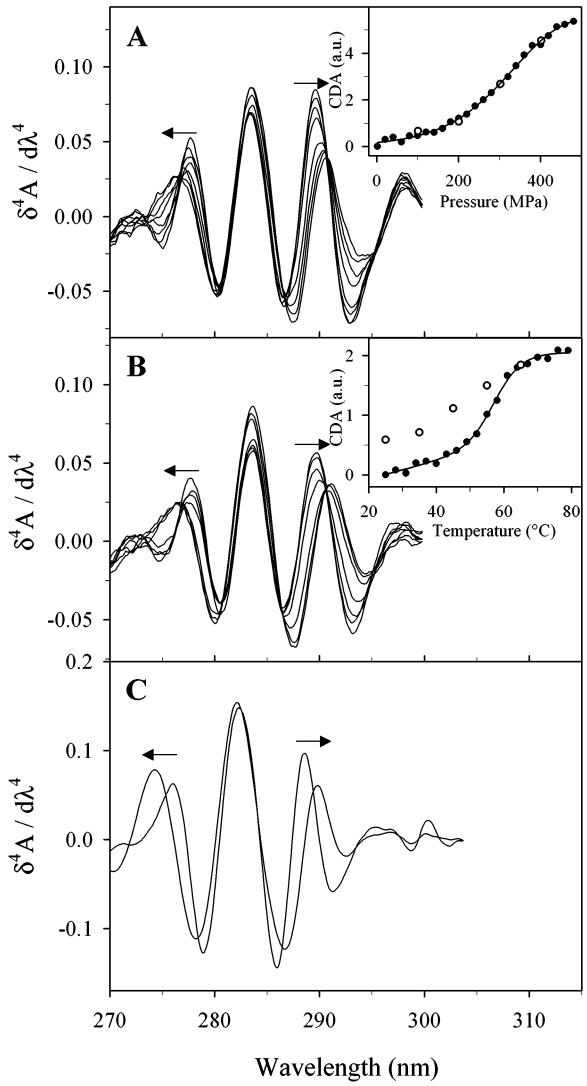

FIGURE 4: Fourth derivative UV absorbance spectra of $SHaPrP_{90-231}$ as a function of pressure (A) and temperature (under 200 MPa) (B) Arrows indicate the spectral shift. Experimental conditions: A, Tris-HCl buffer, 20 mM, pH 7.0, at 40 °C and B, sodium phosphate buffer, 20 mM, pH 7.0, at 200 MPa. The protein concentration was 0.5 mg mL^{-1}. The insets show the change in signal intensity expressed as cumulative difference amplitude (CDA) for increasing (filled circles) and decreasing (open circles) pressure or temperature. The solid lines show nonlinear least-squares fits of the data based on a two-state model. (C) Simulation of the spectral shift (arrows) by spectral superposition of Tyr (*N*-acetyl-tyrosine-O-ethylester) and Trp (*N*-acetyl-tryptophan-O-ethylester) model compounds in solvents of different polarity. Initial condition: Tyr in 25% ethanol + Trp in water; final condition: Tyr in water + Trp in 50% ethanol.

indicating a two-state conformational change. The transitions were thus fitted to a two-state thermodynamic model combined with sloping functions for the native and the nonnative states (*34*). Sigmoidal unfolding profiles were obtained, both probing tyrosine (within the 275−290-nm range), as illustrated in the insets to Figure 4, and probing tryptophan (290−295-nm range). The resulting two-state transitions were virtually identical, suggesting that the Tyr and Trp environments were affected in a cooperative manner. While pressure-induced changes were found to be completely reversible, a small hysteresis was observed as a function of temperature (see insets of Figure 4).

For comparison under the same conditions (40 °C and 200 MPa), ΔG_U values for thermal unfolding were calculated

Table 1: Thermodynamic Parameters of $SHaPrP_{90-231}$[a]

Pressure-Induced Unfolding[b]			
signal	ΔV_U (mL mol^{-1})	$P_{1/2}$ (MPa)	$\Delta G_{U200MPa, 40\,°C}$[c] (kJ mol^{-1})
UV[d]	−31.9 (1.9)	323	3.93
ANS[e]	−34.7 (2.4)	291	4.10

Temperature-Induced Unfolding[b]				
signal	$\Delta S_{T1/2}$ (J mol^{-1} K^{-1})	$\Delta H_{T1/2}$ (kJ mol^{-1})	$T_{1/2}$ (°C)	$\Delta G_{U200MPa, 40°C}$[c] (kJ mol^{-1})
UV	681 (113)	225 (38)	57.8	9.37

[a] Numbers in parentheses are the standard errors of the data. [b] Unfolding transitions obtained upon increasing pressure were carried out at 40 °C. The temperature denaturation profile was recorded at 200 MPa. [c] Free energy of unfolding at 200 MPa and 40 °C. [d] Fourth derivative UV absorbance change (CDA). [e] Change of ANS fluorescence.

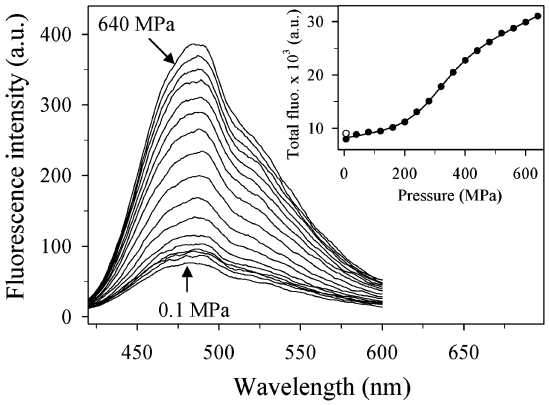

FIGURE 5: Fluorescence emission spectra of ANS in the presence of $SHaPrP_{90-231}$ as a function of pressure. Tris-HCl buffer, 20 mM, pH 7.0, at 40 °C containing 750 μM ANS and 0.8 mg mL^{-1} protein; the excitation wavelength was 350 nm. The inset shows the change in total fluorescence between 420 and 600 nm at increasing pressure (filled circles) and after releasing pressure, at 0.1 MPa (open circle). The solid line is the nonlinear least-squares fit of the data based on a two-state model.

using a constant ΔC_p value (change in heat capacity for the denaturation reaction) of 5.63 kJ K^{-1} mol^{-1}. Since a determination of ΔC_p from the temperature dependence of van't Hoff enthalpy was not possible because of the aggregating processes arising at high temperature, the value for ΔC_p was estimated from the newly accessible surface area exposed to the solvent on unfolding as described previously (*41*). Such an estimation of ΔC_p has been carried out similarly for recombinant human prion protein (*42*). A comparison of the thermodynamic parameters (Table 1) reveals a significant difference in the change of free energy associated with this process: for temperature- and pressure-induced conformational transitions, ΔG_U was 9.4 and 3.9 kJ mol^{-1}, respectively.

Distinctive Structural Features of Pressure-Induced Conformations. For a further characterization of the heat- (at 200 MPa) and pressure-induced conformational states, we studied their ability to bind ANS and thioflavin-T. At high temperature (under 200 MPa or at atmospheric pressure), PrP did not bind ANS or thioflavin-T. In contrast, the pressure-induced conformer showed strong binding to both probes. As shown in Figure 5, applying high pressure led to a gradual increase in the ANS fluorescence intensity. The recovery of initial ANS fluorescence upon pressure release was complete.

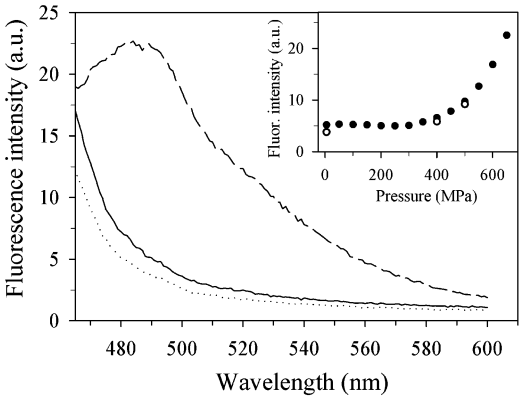

FIGURE 6: Fluorescence emission spectra of thioflavin-T in the presence of $SHaPrP_{90-231}$ at different pressures: 0.1 MPa (solid line), 650 MPa (dashed line), and after releasing pressure to 0.1 MPa (dotted line). The inset shows the total fluorescence intensity between 455 and 600 nm upon increasing pressure. The protein concentration was 0.3 mg mL^{-1} in Tris-HCl buffer, 20 mM, pH 7.0, at 40 °C. Thioflavin-T concentration was 20 μM. The excitation wavelength was 442 nm.

As shown in the inset of Figure 5, the binding curve was sigmoidal, again suggesting a two-state conformational change. The change in free energy (ΔG_U) of this transition was very similar to that of the pressure-induced UV absorbance change (Table 1). In contrast, binding of thioflavin-T occurred at much higher pressures than ANS binding. As shown in Figure 6, at 650 MPa, a still incomplete 5-fold increase in thioflavin-T fluorescence was observed. At higher pH (pH 8.5) and lower temperature (25 °C), this increase in fluorescence was even higher (14-fold). This process was completely reversible, without hysteresis, and did not result in protein aggregation. Control experiments confirmed that this fluorescence enhancement was due to an interaction of thioflavin-T with the prion protein: in the absence of the prion protein, or in the presence of other proteins, no increase in fluorescence was observed.

DISCUSSION

As a tool to study the relationship between macromolecular structure and function, high pressure associated with optical detection (spectroscopic) methods is becoming increasingly popular in biosciences and biotechnology. In the present work, high pressure has been used for the first time as a new approach to study, in vitro, abnormal protein self-assembly processes and particular conformational changes upon unfolding of a mammalian prion protein. Pressure acts specifically on different types of chemical interactions such as hydration of hydrophobic residues, dissociation of charged groups, or stacking of aromatic residues. Pressure appears therefore as a promising new perturbing agent to be used advantageously as an alternative (or a complement) to heat, salts, or chemical denaturants.

High-Pressure Approach to Study Protein Aggregation and Disaggregation. Since amyloid aggregates have been recognized to be a pathological hallmark of several fatal diseases (*43*), protein misfolding and misassembly has attracted a keen interest. Recently, the application of high pressure to proteins associated with amyloid diseases such as lysozyme, transthyretin, or amyloid A protein has gained much attention and is becoming an open and promising research field (*26*). In this study, we demonstrate that pressure offers an elegant

way to avoid the sometimes undesired protein aggregation processes attained in vitro upon increasing temperature, thus enabling the analysis of the heat-induced pathway leading to a soluble unfolded state. Moreover, we present a high-pressure procedure for solubilizing and correctly refolding the PrP aggregates formed at high temperature.

Thermal unfolding of $SHaPrP_{90-231}$, at atmospheric pressure and pH 7.0, is irreversible and results in protein aggregation. These findings are in line with the irreversibility of thermal unfolding reported for $SHaPrP_{90-231}$ (*30*) and $HuPrP_{91-231}$ (*44*), which is also associated with an aggregation process. The aggregates we obtained are characterized by an intermolecular β-sheet-rich structure and the sporadic formation of amyloids. The application of high-pressure reverts this process: the aggregates dissolve, and the initial α-helical secondary structure content is recovered once the pressure is released to atmospheric condition.

To understand such a striking effect of pressure, we have to analyze the molecular events leading to protein aggregation and disaggregation. Upon heating, frequently the hydrophobic core of proteins becomes solvent exposed, and aggregation is due to intermolecular hydrophobic collapse (*45*). Generally, this process is irreversible because of stabilization of an intermolecular network by hydrogen bonds and also sometimes because of chemical alterations such as amino acid degradation due to deamidation, oxidation, and succinimide formation processes (*46*). Pressure can prevent (or reverse) protein aggregation because of its capacity of hydrating hydrophobic residues. Indeed, pressure disaggregation of proteins is not without precedent (*24*−*26*). However, the requirement of chemical denaturants (i.e., guanidinium hydrochloride or urea) in combination with pressure and/or a very long incubation time at high pressure for disaggregation have been reported. In our study, the PrP aggregates formed at high temperature dissolved nearly instantaneously after a sudden increase of pressure (within 100 ms) in the absence of any denaturant.

Insights into Protein Unfolding−*Folding from Combined Use of Pressure and Temperature.* Pressure- or heat-induced protein unfolding is generally reflected by a blue shift of the three major UV fourth derivative bands because of an increased solvent exposure of tryptophan and tyrosine residues (*35*, *47*, *48*). A closer inspection of the derivative spectra as well as the three-dimensional structure of the protein (Figure 7) can explain the unusual results obtained with $SHaPrP_{90-231}$. The 289.6-nm band can be assigned to tryptophan residues in a strongly polar environment (*33*, *34*). Indeed, the two tryptophan residues (99 and 145) are expected to be completely solvent exposed already in the native state (*38*, *39*). Their less polar environment (red shift) under high pressure and high temperature may be explained by an increased interaction with nonpolar residues or by aromatic stacking in the unfolded state. The 277.8-nm band reflects tyrosine, without a significant contribution from tryptophan. Its blue shift of 1.5 nm under high pressure and temperature indicates that the tyrosine residues become more solvent exposed upon protein unfolding. The 283.4-nm band can be attributed mainly to tyrosines in a moderately polar environment (*33*, *34*). From the published NMR structure, we determined that their average degree of burying is 67% in the native state (*38*, *39*). However, this band also contains a small contribution from tryptophan. The observed invariance of this band as a function of pressure and temperature is readily explained by a compensating effect of the red-shifted tryptophans to the blue-shifted tyrosines. It is indeed possible to simulate this effect by superposition of tyrosine and tryptophan spectra in solvents of different polarity (Figure 4C).

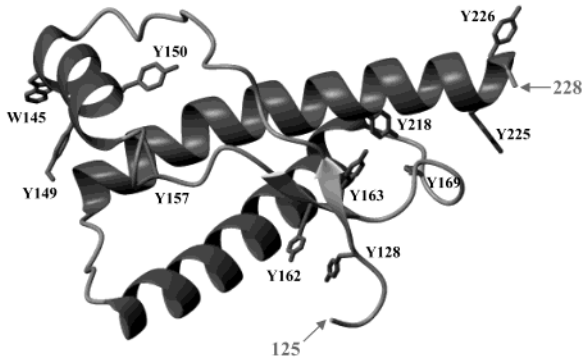

FIGURE 7: Schematic representation of the three-dimensional structure of $SHaPrP_{90-231}$ showing the side chains of the tyrosines and tryptophan residues. An additional Trp residue is located in the region expanding from residues 90−124, which is not shown since marked conformational heterogeneity and structural plasticity was found (*38*, *39*). The figure was produced using the program MOLMOL (*58*).

A comparison with the fourth derivative UV spectrum of the protein at 6 M guanidinium hydrochloride, a condition under which prion proteins are unfolded (*49*, *50*), reveals the same spectral change. This indicates that the UV absorbance changes we observed reflect, at least, partial protein unfolding. However, as shown by the different ΔG_U values, heat- and pressure-induced unfolding processes are not the same: much less energy is needed for pressure-induced unfolding. This suggests that heat and pressure do not lead to identical unfolded structures, an observation that has been made also for other proteins (*19*, *51*−*54*). Indeed, high pressure can be expected to lead to a different unfolded structure than that which can be obtained by other parameters, such as temperature or chemical denaturants. Therefore, pressure appears as an interesting tool to explore new conformational coordinates of the prion protein conformational landscape. Pressure affects protein conformation by promoting the entry of water into the protein structure, thus triggering a chain of events leading to unfolding. In contrast, in the case of temperature, unfolding may take place first, followed by water penetration. High-pressure unfolded states contain frequently residual secondary structure and resemble a compact globule-like state. This particularity of pressure is also reflected in the ANS and thioflavin-T binding properties of the unfolded state: their binding is observed only under high pressure and not at high temperature. However, these two dyes do not bind under the same pressure range. ANS binding occurs with a $P_{1/2}$ of 291 MPa, whereas thioflavin-T starts binding above 400 MPa. The change in free energy evidenced by ANS binding is very similar to that observed by the UV absorbance detection method. This suggests that the unfolded form detected by UV absorbance under high pressure is the same as that which binds ANS. Since ANS is a probe for solvent exposed hydrophobic domains retaining some degree of structure, it is conceivable that the pressure-induced unfolded state (unfolded state 1 in Figure 8) has clusters of hydrophobic side chains that are

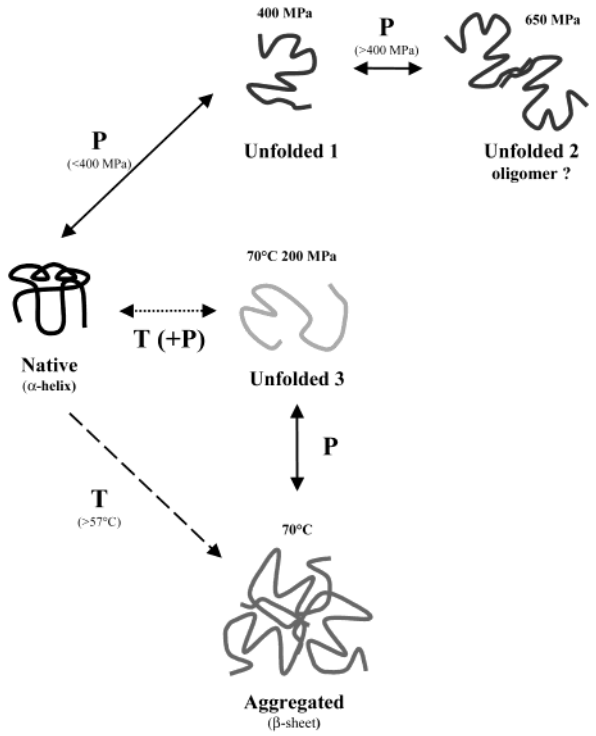

FIGURE 8: Schematic representation of the alternative $SHaPrP_{90-231}$ structural changes revealed by high pressure (P) and high temperature (T).

not yet fully unfolded, thus providing binding sites for the dye. In contrast, the heat induced unfolded state (at 200 MPa) cannot bind ANS (unfolded state 3 in Figure 8), suggesting that it contains a lower level of structural organization.

The binding of thioflavin-T above 400 MPa reveals an additional pressure-induced conformational change from the unfolded state (unfolded state 1) to another structure that has the capacity to bind this dye (unfolded state 2 in Figure 8). Generally, thioflavin-T binding is used as a marker for amyloid structures (*37*). Clearly, this was not the case under our conditions, as the protein remained soluble. However, it is possible that our results reflected the formation of a metastable oligomeric structure at very high pressure. Indeed, thioflavin-T binding to small oligomers has recently been reported (*55*), indicating that binding of this dye is not restricted to amyloid fibrils.

CONCLUSION

The use of high pressure permitted us to study several alternative PrP structural changes, as schematized in Figure 8. Up to 400 MPa, the protein unfolds partly: the tyrosine residues become more exposed on average, and the formerly well-exposed tryptophans interact with nonpolar residues. ANS binding studies revealed the same scenario. At pressures above 400 MPa, the partly unfolded state undergoes a further conformational state, possibly to a metastable oligomeric structure, as revealed by thioflavin-T binding. In addition, pressure assisted heat-induced unfolding (at 200 MPa) leads to a different unfolded structure (different ΔG_U and incapacity of ANS and thioflavin-T to bind). Finally, heat-induced prion aggregation and formation of intermolecular β-sheet structure is reversed by pressure, and pressure-jumps allow studying the kinetics of both aggregation and disaggregation. Some of these conformational changes, which are revealed by our high-pressure approach, may also have a biological relevance. Indeed, recent modeling studies suggest the existence of multiple folding−unfolding pathways for prion proteins (*56*, *57*). Our results show that the use of high pressure gives the possibility to explore the energetic and conformational landscape of these structural changes. This original tool may reveal to be helpful in screening for various ligands such as nucleic acids, heat shock proteins, or sulfated glycosaminoglycans that may modulate these processes.

ACKNOWLEDGMENT

We gratefully acknowledge B. Calas for carrying out ES/MS analysis of $SHaPrP_{90-231}$, L. Chiche for computing its solvent accessibility, C. Valentin for expert technical assistance in high-pressure experiments, and J. A. Kornblatt and M. J. Kornblatt for helpful discussions. We also thank S. B. Prusiner for the gift of a plasmid containing the gene encoding $SHaPrP_{90-231}$.

REFERENCES

1. Prusiner, S. B. (1998) *Proc. Natl. Acad. Sci. U.S.A. 95*, 13363−13383.
2. Prusiner, S. B., Scott, M. R., DeArmond, S. J., and Cohen, F. E. (1998) *Cell 93*, 337−348.
3. Caughey, B. (2001) *Trends Biochem. Sci. 26*, 235−242.
4. Cohen, F. E. (1999) *J. Mol. Biol. 293*, 313−320.
5. Baskakov, I. V., Aagaard, C., Mehlhorn, I., Wille, H., Groth, D., Baldwin, M. A., Prusiner, S. B., and Cohen, F. E. (2000) *Biochemistry 39*, 2792−2804.
6. Swietnicki, W., Morillas, M., Chen, S. G., Gambetti, P., and Surewicz, W. K. (2000) *Biochemistry 39*, 424−431.
7. Baskakov, I. V., Legname, G., Prusiner, S. B., and Cohen, F. E. (2001) *J. Biol. Chem. 276*, 19687−19690.
8. Nandi, P. K., Leclerc, E., and Marc, D. (2002) *Biochemistry 41*, 11017−11024.
9. Zhou, J. M., Zhu, L., Balny, C., and Perrett, S. (2001) *Biochem. Biophys. Res. Commun. 287*, 147−152.
10. Weber, G. (1992) *Protein interactions*, pp 199−215, Chapman and Hall, London.
11. Balny, C., Masson, P., and Heremans, K., Eds. (2002) *Frontiers in High-Pressure Biochemistry and Biophysics*, Elsevier, Amsterdam.
12. Smeller, L., Rubens, P., and Heremans, K. (1999) *Biochemistry 38*, 3816−3820.
13. Ruan, Q., Ruan, K., Balny, C., Glaser, M., and Mantulin, W. W. (2001) *Biochemistry 40*, 14706−14714.
14. Ikeuchi, Y., Suzuki, A., Oota, T., Hagiwara, K., Tatsumi, R., Ito, T., and Balny, C. (2002) *Eur. J. Biochem. 269*, 364−371.
15. Meersman, F., Smeller, L., and Heremans, K. (2002) *Biophys. J. 82*, 2635−2644.
16. Peng, X., Jonas, J., and Silva, J. L. (1993) *Proc. Natl. Acad. Sci. U.S.A. 90*, 1776−1780.
17. Prevelige, P. E., Jr., King, J., and Silva, J. L. (1994) *Biophys. J. 66*, 1631−1641.
18. Clery, C., Renault, F., and Masson, P. (1995) *FEBS Lett. 370*, 212−214.
19. Zhang, J., Peng, X., Jonas, A., and Jonas, J. (1995) *Biochemistry 34*, 8631−8641.
20. Vidugiris, G. J., and Royer, C. A. (1998) *Biophys. J. 75*, 463−470.
21. Kobashigawa, Y., Sakurai, M., and Nitta, K. (1999) *Protein Sci. 8*, 2765−2772.
22. Chapeaurouge, A., Johansson, J. S., and Ferreira, S. T. (2001) *J. Biol. Chem. 276*, 14861−14866.
23. Mozhaev, V. V., Heremans, K., Frank, J., Masson, P., and Balny, C. (1996) *Proteins 24*, 81−91.
24. Silva, J. L., Foguel, D., and Royer, C. A. (2001) *Trends Biochem. Sci. 26*, 612−618.
25. Perrett, S., and Zhou, J. M. (2002) *Biochim. Biophys. Acta 1595*, 210−223.
26. Randolph, T. W., Seefeldt, M., and Carpenter, J. F. (2002) *Biochim. Biophys. Acta 1595*, 224−234.

27. Gorovits, B. M., and Horowitz, P. M. (1998) *Biochemistry 37*, 6132−6135.
28. St. John, R. J., Carpenter, J. F., Balny, C., and Randolph, T. W. (2001) *J. Biol. Chem. 276*, 46856−46863.
29. Mehlhorn, I., Groth, D., Stockel, J., Moffat, B., Reilly, D., Yansura, D., Willett, W. S., Baldwin, M., Fletterick, R., Cohen, F. E., Vandlen, R., Henner, D., and Prusiner, S. B. (1996) *Biochemistry 35*, 5528−5537.
30. Zhang, H., Stockel, J., Mehlhorn, I., Groth, D., Baldwin, M. A., Prusiner, S. B., James, T. L., and Cohen, F. E. (1997) *Biochemistry 36*, 3543−3553.
31. Byler, D. M., and Susi, H. (1986) *Biopolymers 25*, 469−487.
32. Kitamura, Y., and Itoh, T. (1987) *J. Sol. Chem. 16*, 715−725.
33. Lange, R., Frank, J., Saldana, J. L., and Balny, C. (1996) *Eur. Biophys. J. 24*, 277−283.
34. Lange, R., Bec, N., Mozhaev, V. V., and Frank, J. (1996) *Eur. Biophys. J. 24*, 284−292.
35. Torrent, J., Connelly, J. P., Coll, M. G., Ribo, M., Lange, R., and Vilanova, M. (1999) *Biochemistry 38*, 15952−15961.
36. Engelhard, M., and Evans, P. A. (1995) *Protein Sci. 4*, 1553−1562.
37. LeVine, H., III (1993) *Protein Sci. 2*, 404−410.
38. James, T. L., Liu, H., Ulyanov, N. B., Farr-Jones, S., Zhang, H., Donne, D. G., Kaneko, K., Groth, D., Mehlhorn, I., Prusiner, S. B., and Cohen, F. E. (1997) *Proc. Natl. Acad. Sci. U.S.A. 94*, 10086−10091.
39. Liu, H., Farr-Jones, S., Ulyanov, N. B., Llinas, M., Marqusee, S., Groth, D., Cohen, F. E., Prusiner, S. B., and James, T. L. (1999) *Biochemistry 38*, 5362−5377.
40. Tamm, L. K., and Tatulian, S. A. (1997) *Q. Rev. Biophys. 30*, 365−429.
41. Myers, J. K., Pace, C. N., and Scholtz, J. M. (1995) *Protein Sci. 4*, 2138−2148.
42. Swietnicki, W., Petersen, R. B., Gambetti, P., and Surewicz, W. K. (1998) *J. Biol. Chem. 273*, 31048−31052.
43. Dobson, C. M. (2002) *Nature 418*, 729−730.
44. Jackson, G. S., Hill, A. F., Joseph, C., Hosszu, L., Power, A., Waltho, J. P., Clarke, A. R., and Collinge, J. (1999) *Biochim. Biophys. Acta 1431*, 1−13.
45. Jaenicke, R., and Seckler, R. (1997) *Adv. Protein Chem. 50*, 1−59.
46. Daniel, R. M., Dines, M., and Petach, H. H. (1996) *Biochem. J. 317* (*Pt 1*), 1−11.
47. Mombelli, E., Afshar, M., Fusi, P., Mariani, M., Tortora, P., Connelly, J. P., and Lange, R. (1997) *Biochemistry 36*, 8733−8742.
48. Ruan, K., Xu, C., Yu, Y., Li, J., Lange, R., Bec, N., and Balny, C. (2001) *Eur. J. Biochem. 268*, 2742−2750.
49. Hornemann, S., and Glockshuber, R. (1996) *J. Mol. Biol. 261*, 614−619.
50. Swietnicki, W., Petersen, R., Gambetti, P., and Surewicz, W. K. (1997) *J. Biol. Chem. 272*, 27517−27520.
51. Takeda, N., Kato, M., and Taniguchi, Y. (1995) *Biochemistry 34*, 5980−5987.
52. Heremans, K., and Smeller, L. (1997) *Eur. J. Solid State Inorg. Chem. 34*, 745−758.
53. Chatani, E., Nonomura, K., Hayashi, R., Balny, C., and Lange, R. (2002) *Biochemistry 41*, 4567−4574.
54. Lesch, H., Stadlbauer, H., Friedrich, J., and Vanderkooi, J. M. (2002) *Biophys. J. 82*, 1644−1653.
55. Carrotta, R., Bauer, R., Waninge, R., and Rischel, C. (2001) *Protein Sci. 10*, 1312−1318.
56. Locker, C. R., and Hernandez, R. (2001) *Proc. Natl. Acad. Sci. U.S.A. 98*, 9074−9079.
57. Levy, Y., and Becker, O. M. (2002) *Proteins 47*, 458−468.
58. Koradi, R., Billeter, M., and Wuthrich, K. (1996) *J. Mol. Graph. 14*, 51−55.

BI0269916